IOPscience iopscience.iop.org

Home Search Collections Journals About Contact us My IOPscience

Stretchable polyurethane sponge reinforced magnetorheological material with enhanced mechanical properties

This content has been downloaded from IOPscience. Please scroll down to see the full text.

2015 Smart Mater. Struct. 24 037001

(http://iopscience.iop.org/0964-1726/24/3/037001)

View the table of contents for this issue, or go to the journal homepage for more

Download details:

IP Address: 218.22.21.3
This content was downloaded on 06/02/2015 at 15:17

Please note that terms and conditions apply.

IOP Publishing Smart Materials and Structures
Smart Mater. Struct. **24** (2015) 037001 (8pp) doi:10.1088/0964-1726/24/3/037001

Technical Note

Stretchable polyurethane sponge reinforced magnetorheological material with enhanced mechanical properties

Lin Ge, Shouhu Xuan, Guojiang Liao, Tiantian Yin and Xinglong Gong

CAS Key Laboratory of Mechanical Behavior and Design of Materials, Department of Modern Mechanics, University of Science and Technological of China, Hefei, 230027, People's Republic of China

E-mail: gongxl@ustc.edu.cn and xuansh@ustc.edu.cn

Received 20 August 2014, revised 17 November 2014
Accepted for publication 19 November 2014
Published 3 February 2015

Abstract

A stretchable magnetorheological material (SMRM) consisting of micro-meter carbonyl iron (CI) particles, low cross-linking polyurethane (PU) polymer and porous PU sponge has been developed. Due to the presence of the PU sponge, the high-performance MR material can be reversibly stretched or bent, just as MR elastomers. When the CI content increases to 80 wt%, the magnetic induced modulus of the MR material can reach as high as 7.34 MPa and the corresponding relative MR effect increases to 820%. A possible strengthening mechanism of the SMRM was proposed. The attractive mechanical properties make the SMRM a promising candidate for future high-performance devices.

Keywords: magnetorheological, 3D network supporting, polyurethane sponge

(Some figures may appear in colour only in the online journal)

1. Introduction

Flexible, highly sensitive, quick-responding, and environmentally friendly magnetorheological (MR) materials are highly desired in future generations of shock absorption and noise reduction devices, such as the adaptive tuned vibration absorbers, mass dampers, sensors, actuators, base isolator, etc [1–5]. The MR materials are classified into MR elastomers [6], MR foams [7], MR fluids [8], MR gels [9], and so on. Traditional MR fluids and MR gels are flexible, but have the problems of particle deposition, environmental contamination, sealing, etc [10–12]. The MR elastomers were developed by fixing the carbonyl iron (CI) particles in the polymer matrix to avoid particle deposition and sealing. However, the CI particles in the matrix are hard to move while applying an external magnetic field. As a result, it is difficult to obtain MR elastomers with a high magnetic-induced modulus and MR effect. MR plastomer [13, 14], a newly developed MR material, has been paid great attention owing to its specific properties, including feasible preparation, flexibility, high magnetic-induced modulus, and high MR effect. Unfortunately, the strain generated by the active materials during the stretch or bend cannot exceed the levels of induced fracture limits and the shape cannot recover after deformation. As a result, a much more challenging device that can flex, stretch, or randomly bend like MR elastomers but with a much higher MR performance is urgently needed.

Recently, three-dimensional (3D) material such as porous sponge and foam works as a scaffold has been introduced to the smart material to enhance the mechanical properties [15–22]. In these novel 3D structured functional materials, the interconnected bone structure can work as a skeleton to maintain elasticity and withstand the tensile stress. For example, Jeong *et al* [23] prepared a high-performance electrode by electroplating noble metal on 3D porous polydimethylsiloxane (PDMS) that was fabricated by applying pressurized steam to an uncured PDMS surface. The 3D porous PDMS supported the electroplated metal stably while randomly stretching. Yao *et al* [24] designed a pressure sensor by coating the 3D porous polyurethane (PU) sponge

 © 2015 IOP Publishing Ltd Printed in the UK

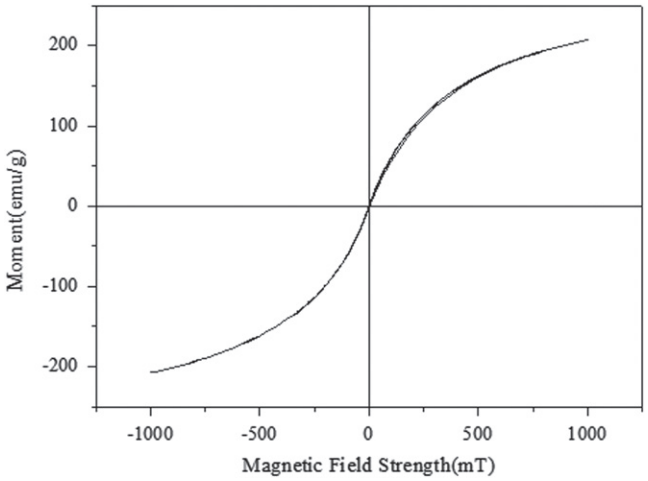

Figure 1. VSM data for CI particles of type CN.

with a thin layer of conductive graphene. The sponge works as a bendable, elastic, and perfect beam and can be reversibly pressed for thousands of times. Similarly, by wrapping AgNWs (silver nanowires) on a micro-scale PU sponge scaffold [25], a binary composite with typical flexibility, stretchability, and stress-dependent conductivity can be successfully obtained. Clearly, this kind of 3D matrix works as a bone structure that can integrate the separate section into cohesive and interactive devices.

3D material also can be utilized in preparing MR materials due to its unique properties. Foam devices with constrained MR fluid in a porous matrix such as a sponge, open-celled foam, felt, or fabric have been developed [10]. Under the magnetic field, the matrix can keep the MR fluid located in the active region of the devices. Scarpa *et al* [26] reported a novel class of auxetic rigid PU MR foam by coating a PU sponge with MR fluid. An auxetic solid expands in all directions when pulled in only one, thus behaving in an opposite manner compared to 'classical' solids. Gong *et al* [7] oriented the CI particles in the liquid polyol to form a chain-like structure by using an external magnetic field, and then the chain-like structures were fixed in the PU foam after the *in situ* polymerization. The maximum magnetic-induced modulus of the anisotropic porous MR foam was 1.07 MPa and the relative MR effect was 27.1%. To our knowledge, these newly developed flexible MR materials containing a 3D network present possibilities in absorber and sensor, but their low magnetic-induced modulus and MR effect limit their practical application.

In this work, a novel high-performance stretchable magnetorheological material (SMRM) was reported by interpreting a low cross-linking PU-based MR plastomer into the pores of a commercial low-density PU sponge. The geometrical characteristics can significantly affect the stress distribution in the fiber/matrix composites [27]. So the PU sponge works as a skeleton to reinforce the MR plastomer and the as-prepared SMRM exhibits high MR effects than the traditional MREs (magnetorheological elastomers) and MR plastomers. Due to the presence of the elastic micro-meter scale, interconnected, and porous PU sponge, this novel MR material exhibits stretchable, flexible, and elastic characteristics. The main contribution of this work is to experimentally investigate the magnetorheological response of the SMRM for possible application in vibration absorbers, mass dampers, actuators, base isolators, etc. Both the magnetic-induced modulus and the loss factor, which are the most important factors for good actuators and dampers, are presented in this technical note.

2. Experimental

2.1. Raw materials

Toluene diisocyanate (TDI; 2,4 ≈ 80%, 2,6 ≈ 20%) and polypropylene glycol (PPG-2000, Mn = 2000) purchased from Anhui Anda Huatai Xincailiao Co., Ltd, China were selected as the main reagents. 1, 4-butanediol (BDO) purchased from Sinopharm Chemical Reagent Co., Ltd China, was used as chain extender. The magnetic particles were CI particles (type CN) provided by BASF in Germany with an approximate size of 7 μm. The VSM (vibrating sample magnetometer) data of CI particles was shown in figure 1. The values of the saturation magnetization and coercivity were 207.34 emu g^{-1} and 0.09 A M^{-1}, respectively. Therefore, the CI particles exhibited a typical soft magnetic characteristic. The magnetization of CI particles increased as the magnetic field became stronger. A commercially available low-density PU sponge with 3D-interconnected microfiber networks was used as a skeleton to construct the stretchable PU sponge-reinforced MR composite. The apparent core density of the sponge was 16.56 kg m^{-3}, which was tested according to GB/T 6343-2009. The total volume of the pores of the neat sponge is 91.2%, and the apparent volume of the sponge V_a was tested according to GB/T 6342-1996. The volume of the sponge filament V_f was achieved by inserting the sponge into the alcohol in a measuring cylinder. The total volume of the pores of the neat sponge is (V_a- V_f)/ V_a.

2.2. Sample preparation

The preparation of SMRM was composed of three steps. First, uncross-linking PU was prepared by homogeneously mixing TDI and PPG in a 250- mL, three-necked, round-bottom flask with a stirrer, agitating for 2 h at 80 °C. BDO was added after cooling down the reaction system below 40 °C. Then, the low-cross-linking PU was transferred into a beaker and the CI particles were added into the precursor by vigorously stirring until the polymer and iron particles were well mixed. In this work, the weight content of the CI particles according to the PU varied from 40 wt% to 60 wt%, 70 wt%, and 80 wt%. Finally, the PU sponge, which was cut into pieces with a diameter of 20 mm and 1 mm in thickness, was totally dipped into the PU-CI mixture. After incorporating with the PU sponge, the CI content of the SMRM sample turned into 39.7%, 59.7%, 69.8%, and 79.8%, respectively. The low-density PU sponge was about 0.005 g for each piece. The

mass of the sponge had been calculated in the CI content calculation and regarded the CI content of SMRM as 40%, 50%, 60%, and 70% as well in the following work. Owing to the unique micro-meter scale, interconnected, and porous structure, the PU sponge was infiltrated with the MR precursor under capillary forces. The PU sponge turned black because the holes of the sponge were filled with the PU-CI precursor. After the sample was placed at room temperature for 72 h, SMRM was successfully achieved. The size of the final SMRM is the same as the PU sponge, with 20 mm in diameter and 1 mm in thickness. By way of contrast, the samples without the PU sponge were also prepared to investigate the strengthening effects.

2.3. Properties characterization

The microstructure of the SMRM was observed by an environmental scanning electron microscope (SEM, Philips of Holland, model XT30 ESEM-MP). The accelerating voltage was 20 KV. A thin layer of gold was coated on the transection of the sample. The microstructure of the PU sponge and the SMRM was studied.

In order to have a better application in shock absorption and noise reduction devices, dynamic properties of the samples were characterized by a commercial rheometer (Physica MCR 301, Anton Paar Co., Austria). The sample was placed between the paralleled rotating disc and the base. The current applied to the electromagnetic coil generated a magnetic field. The magnetic field strength was controlled by the magnitude of the electric current. The direction of the magnetic field was paralleled with the thickness of the sample. A pre-pressure was exerted on the sample to prevent the sample from sliding on the disk. The test was in shear oscillation mode. The shear strain amplitude was 0.1% (making sure the testing data falls in the linear viscoelastic region) and the frequency was 5 Hz. The temperature was controlled by circulating water set at 25 °C. The magnetic field strength sweep was from 0 mT to 1000 mT.

The tensile strength was tested by Material Test System (MTS) (MTS criterion 43, MTS System Co., America). The sample was cut into 2 mm × 30 mm × 60 mm pieces, and the test area was 2 mm × 30 mm × 40 mm. The sample was held by a clamp, and the stretching rate was 1 mm min^{-1}.

3. Results and discussion

3.1. Synthesis and microstructure of SMRM

As soon as the low-cross-linking PU was achieved, the CI particles were introduced and mixed homogeneously. Then, the precursor was integrated into the PU sponge skeleton to construct the SMRM. Owing to the unique macro-porous structure, each micro-hole of the sponge was fully filled with the PU-CI precursor, and the whole sample turned black (figure 2(a)). Because of the high stability and elasticity, the final SMRM exhibited much better mechanical properties than conventional MRPs and MREs. In the absence of the magnetic field, the CI particles spread homogeneously in the matrix and no particle aggregation was clearly found in the optical microscope images (figures 2(b)~(f)). When an external magnetic field was applied to the samples, the CI particles began to move and formed a linear structure (figure 2(c)) along the direction of the magnetic field. The schematic mechanism of the stretchable composite MR materials was shown in figure 2(g).

The SEM was used to investigate the microstructure of the PU sponge bone structure and the SMRM. The PU sponge is a 3D porous network, and the pores interconnect with each other (figure 3(a)). The width of interconnected channels (figure 3(b)) generally ranges from 30 μm to 60 μm. The matrix formed by the PU precursor and PU sponge is shown in figure 3(c). It is hard to distinguish the PU sponge from the PU precursor, as they were well combined together. The cutting surface is rough and bumpy. The CI particles are dispersed homogeneously in the polymer matrix (figure 3(d)), so it is hard to distinguish the PU sponge from the SMRM. Because the CI particles are movable in the PU matrix, the relative MR effect of this kind of SMRM is higher than MREs.

3.2. Dynamic properties of the SMRM

It is feasible to tune the dynamic properties of the SMRM by controlling the content of the CI particles in the PU-CI precursor. Here we introduce four kinds of CI weight fraction SMRMs: 40 wt%, 60 wt%, 70 wt%, and 80 wt%. The dynamic properties are mainly characterized by shear storage modulus (G') and loss factor. The relationship between G' and magnetic field strength of the SMRM is shown in figure 4. For G' of SMRM, it shows an increasing tendency and approaches a maximum value with the increase of the magnetic field, similar to the conventional MREs. The CI content exhibits a great impact on G' of SMRM. The G' increases as the CI content increases. By varying the CI particle content from 0 wt% to 40 wt%, 60 wt%, 70 wt%, and 80 wt%, the zero field modulus (G_0) of SMRM changes from 0.04 to 0.21, 0.23, 0.30, and 0.90 MPa, respectively, which indicates the CI particles strengthen the matrix. On the other hand, by increasing the CI content, the distance between the CI particles reduces; thus, the strong dipole-dipole interaction among the adjacent magnetic particles leads to the formation of robust CI columns [28]. As a result, the magnetic saturation modulus (G_{max}) of the composite MR materials is saturated at 0.04, 3.72, 5.72, 6.19, and 8.24 MPa, respectively. Loss modulus (G'') of the samples was also investigated. From figure 4, it can be found that G'' increases as the magnetic field strength increases within 100 mT. When the magnetic field is applied, the CI particles are reassembled, and this led to the increase of energy dissipation. However, if the magnetic field is increased from 100 to 500 mT, the change of G'' reversed because the sample with the higher CI content was realigned. From 500 to 1000 mT, G''decreases as the magnetic field increases. The thinner linear structure with lower CI particles are easily destroyed by the shear stress and then realign quickly under the magnetic field. The sliding friction

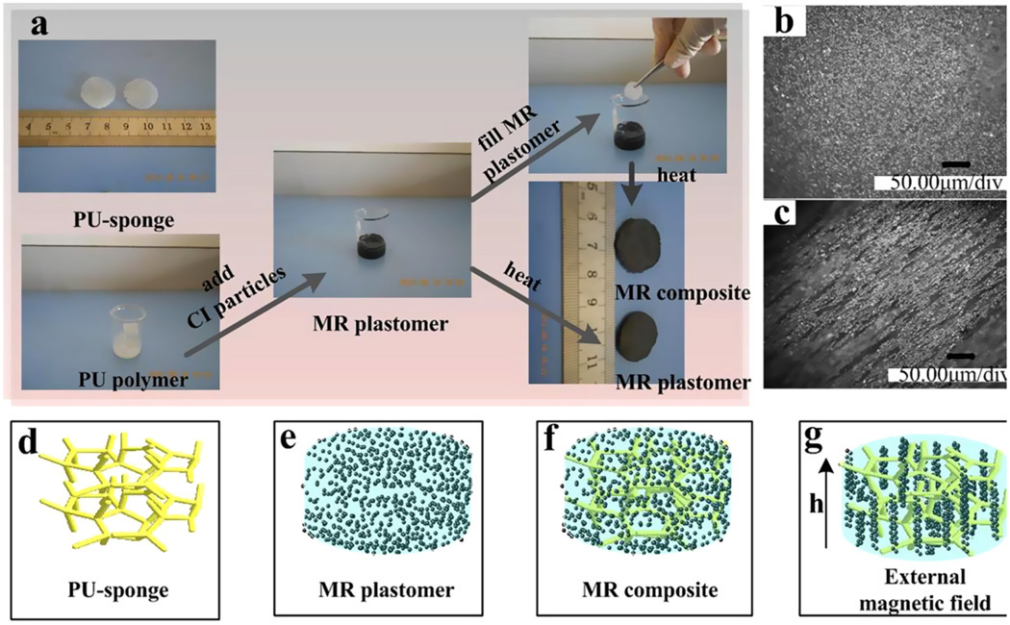

Figure 2. (a) Fabrication procedure of SMRM. (b) Optical microscope images of isotropic SMRM fracture surface. (c) Optical microscope images of anisotropic SMRM fracture surface. (d)~(g) Schematic illustration for the SMRM. (d) The PU sponge. (e) The plastic MR material. (f) The fabricated composite material. (g) The linear structure formed under an external magnetic field.

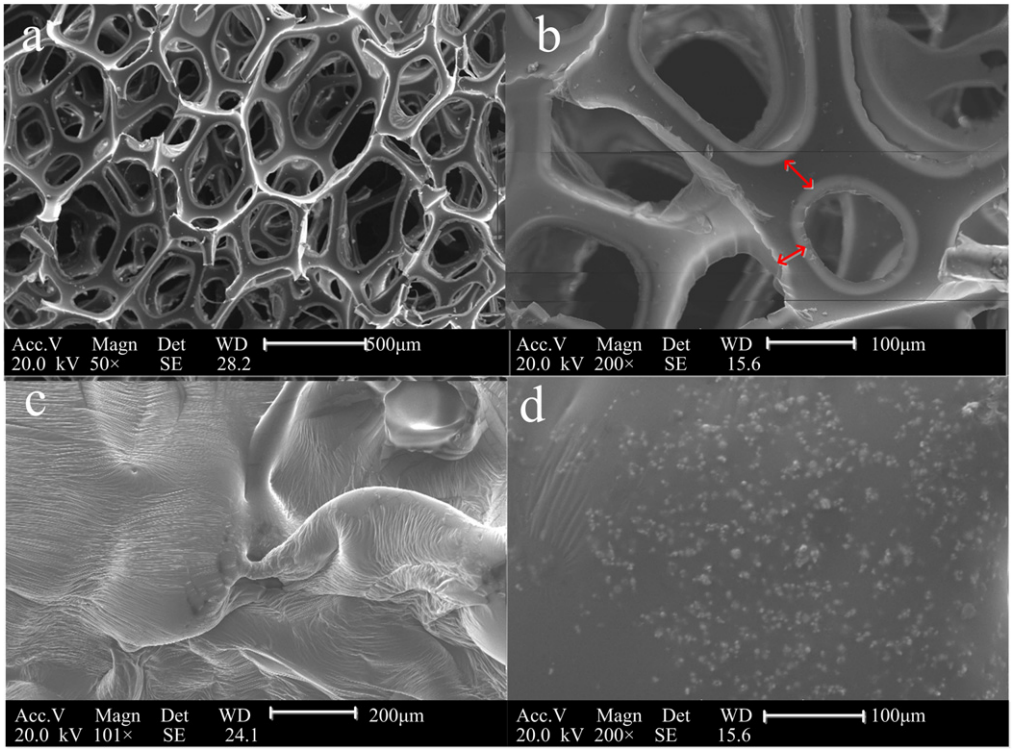

Figure 3. SEM images of the samples: (a) microstructure of PU sponge; (b) microstructure magnification of PU sponge; (c) the matrix; (d) isotropic SMRM.

between the CI particles and the matrix was much larger than the stronger linear structure with more CI particles, so more energy was dissipated.

The ΔG increases with the CI content (table 1), while the MR effects decrease gradually. For example, by increasing the CI content from 60 wt% to 70 wt%, 80 wt%, the MR effect decreases from 2373% to 1980%, 820%. The higher CI content leads to the higher G_0; thus, the MR effect decreases in response to CI content. With a low CI content, the CI particles have good movability in matrix and they can move easily between the holes of the PU sponge under the magnetic field. If the CI content is higher, the CI particles are restricted

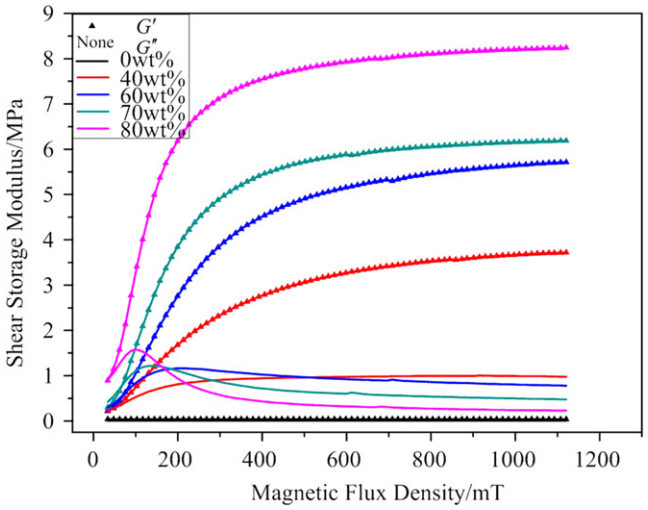

Figure 4. Shear storage modulus (G') and loss modulus (G'') of the sample with different contents of CI particles under different magnetic field strengths.

Table 1. Influence of CI contents to zero field modulus (G_0), magnetic-induced modulus (ΔG), and relative MR effect.

CI content	G_0/MPa	ΔG/MPa	Relative MR effect/%
40 wt%	0.21	3.51	1650
60 wt%	0.23	5.49	2373
70 wt%	0.30	5.89	1980
80 wt%	0.90	7.34	820

in the holes due to the friction. The bone of the PU sponge can help prevent the linear structure from breaking down, so the SMRM possesses high ΔG.

The MRPs, by contrast, show a high MR effect, and the ΔG can reach as high as 6.25 MPa (table 2) when the CI content is 80%. After introducing the PU sponge as a scaffold, the sponge strengthens the composite material. The sponge and the plastic PU have a good compatibility and work well as a single matrix (figure 3(c)) because both are made of PU. The CI particles in the matrix formed in linear structures (figure 2(c)) when an external magnetic field is exerted. The sponge then helps support the linear structure and prevents it from breaking down when a shear force is applied. So the composite MR material possesses a much higher MR effect and the magnetic-induced modulus can reach as high as 7.34 MPa when the CI content is 80%. Since the PU sponge is elastic, it helps the sample recover quickly from deformation.

The loss factor of the SMRM is shown in figure 5. The change of loss factor shows two stages: the sharper down stage, when the CI particles quickly arrange into a linear structure under the external magnetic field, and the flat stage, when they are saturated. In the first stage, the energy dissipation mainly comes from the sliding friction between the PU matrix and the CI particles. The CI particles moved fast to align under the magnetic field, and the relative displacement between CI particles is huge. As the linear structure becomes

Table 2. Magnetic-induced modulus and MR effect of SMRM and contrast MRP.

Mechanical properties	MR composite	MRP
Magnetic-induced modulus (MPa)	7.34	6.25
MR effect	820%	912%

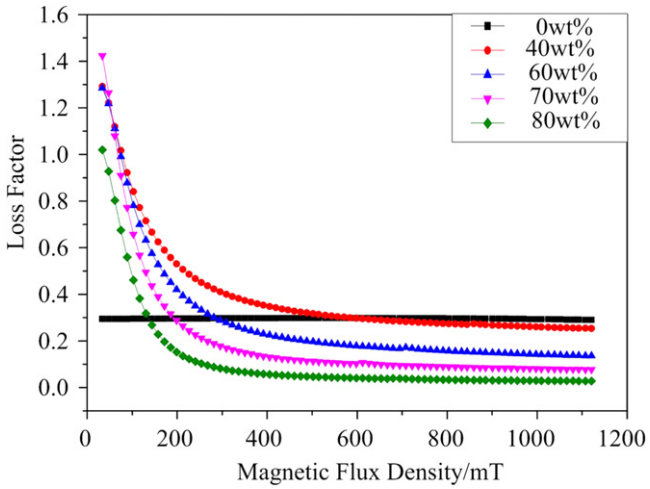

Figure 5. Loss factor of the isotropic SMRM with different CI content under different magnetic field strength.

clearer and stronger, the relative displacement becomes smaller. So the loss factor presents a sharper down stage. On the second stage, all the CI particles are saturated, the linear structure is stable, and the CI particles can hardly move. The energy dissipation mainly comes from the movement of soft segments in the PU matrix. The loss factor of the neat matrix shows a constant value of 0.29. If the CI content is higher, the soft segments are separated by the CI particles; thus, the interaction between the segments becomes weaker. As a result, the sliding friction between the soft segments decreases. The damping of the composite MR materials with the CI particle content of 40 wt%, 60 wt%, 70 wt%, and 80 wt% is 0.25, 0.14, 0.08, and 0.03, respectively. Clearly, as the CI content increases, the impact factor decreases.

To further investigate the working mechanism of this novel SMRM, a binary network model is proposed in figure 6. The model illustrates the shape deformation and the recovery mechanism of the high-performance composite MR materials. As shown in figure 6, shape deformation was generated when a tensile stress was applied on the sample. The PU sponge elongated in the direction of stress and shrank perpendicular to the stress direction (figure 6(d)). After the stress was released, the SMRM completely recovered to its original shape within 30 seconds because of the shrinkage of the PU sponge. However, the contrast MRP cannot sustain a fixed shape. It can be seen from figure 6(c) that the sample can hardly recover after the shape deformation. Thus, the SMRM will hopefully replace MREs in vibration control devices. The flexibility of the matrix contributes to the high magnetic-induced modulus and MR effect, while shape

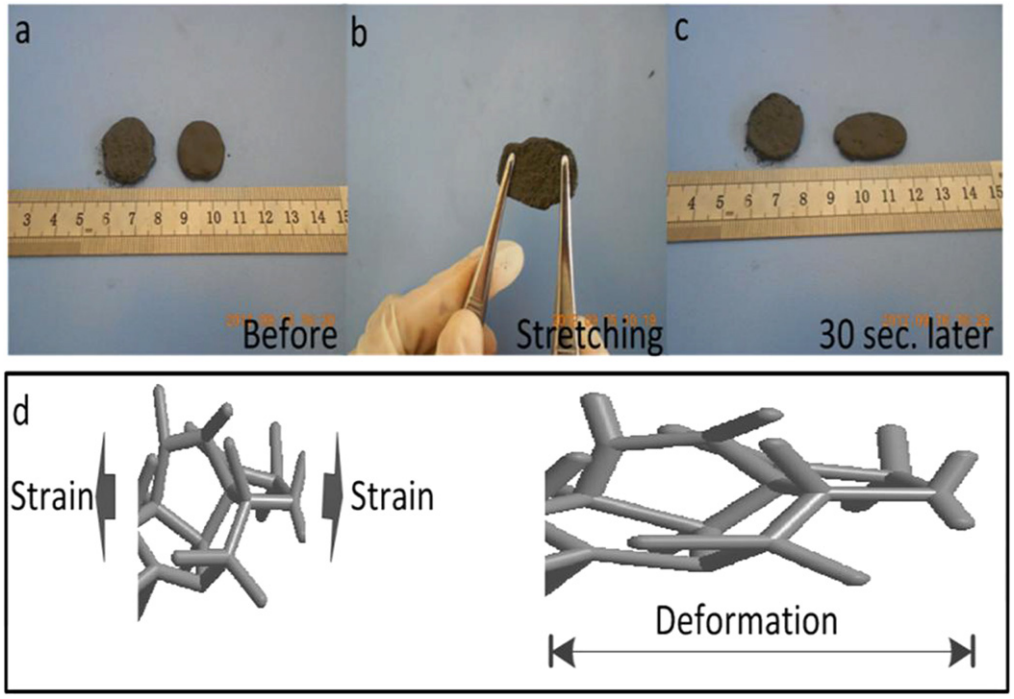

Figure 6. Shape deformation and recovery of the SMRM and MRP.

recovery due to the shrinkage of the PU sponge expands the use of new composite MR materials in many aspects.

Figure 7 shows the tensile strength of the sample with 70 wt% CI. The sample can be easily stretched and bent by using MTS. When the strain ranges from 0% to 25%, the strain-stress curve presents a straight line, so the sample is suffering an elastic deformation. It can be found that the sample was a typically elastic composite. From 25% to 32%, the sample suffered plastic deformation, which means the sample was broken down after elastic deformation. Finally, the sample was destroyed by the tensile stress.

The shear storage modulus of the SMRM and the contrast MRP were studied carefully to show the influence of the PU sponge on the composite material (figure 8(a)). When CI content is 80 wt%, ΔG of the SMRM and contrast MRP are 7.34 MPa and 6.25 MPa (table 2). A good MR material must have a high magnetic-induced modulus, so the G' should change in a wide range. The results show that the composite MR material has a much better mechanical property than the contrast MRP. The elastic PU sponge can help support the linear structure and prevent it from breaking down while applying a shear stress on the MR material. Therefore, the PU sponges contribute to a stronger linear structure, which can bear a larger shear force. Because the PU sponge strengthens the sample and increases the G_0, the MR effect of the SMRM (820%) is a little smaller than the contrast MRP (912%). However, the PU sponge has a huge impact on G' of the samples, the G_{max} of SMRM can reach as high as 8.24 MPa when the PU sponge is introduced. To this end, it is predicted that the SMRM will have a wider application.

Figure 9 illustrates the working mechanism of the SMRM. From the image, we can see that the CI particles spread homogeneously in the matrix and they will quickly

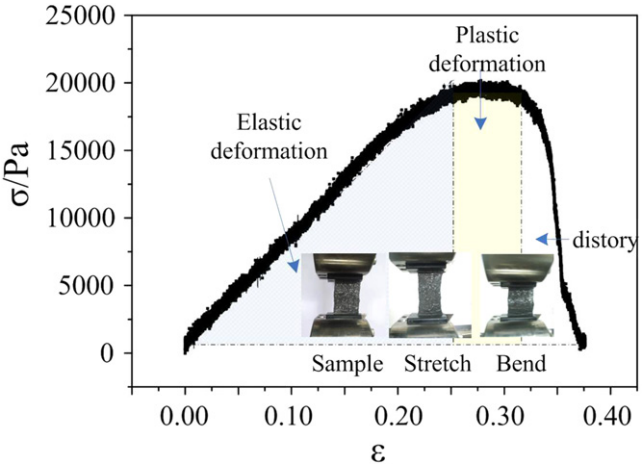

Figure 7. Tensile strength of sample with 70 wt% CI content.

form a linear structure under the magnetic field. The PU sponge stretched in the direction of the linear structure under the magnetic field strength, so the bone perpendicular to the linear structure was pulled taut. The pulled taut bone structure can hardly shift because the sponge was a 3D network. When a shear force was applied on the sample, the linear structure suffered a deformation before yielding. At the same time, the bone structure helps prevent the linear structure from breaking down. The sponge significantly affects the stress distribution in the SMRM while sustaining a shear stress. As a result, the PU sponge can help support the linear structure and increase the shear storage modulus.

The influence of the PU sponge on the loss factor of the SMRM and the contrast MRP were also studied carefully (figure 8(b)). The loss factor curve of the composite MR

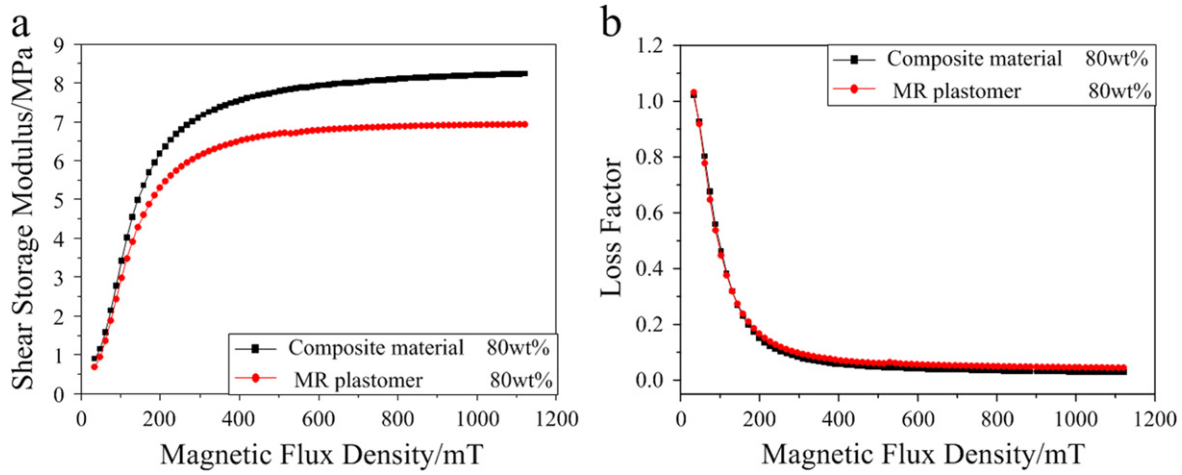

Figure 8. Shear storage modulus and loss factor of the SMRM and the contrast MRP.

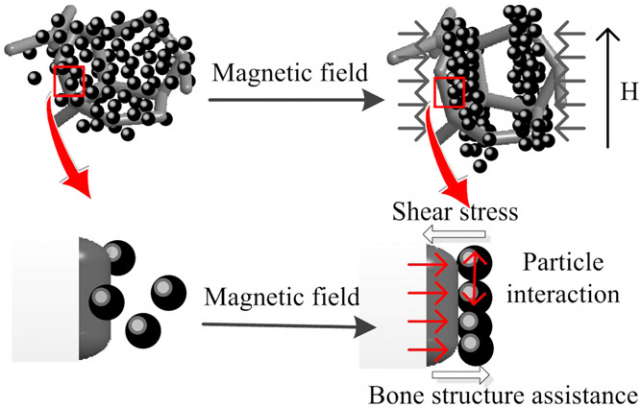

Figure 9. Mechanism of the PU sponge working as a bone structure assistance system and the interaction between particles.

material is quite similar to the MRP. The PU sponge has little influence on the damping property of the same magnetic field because both the sponge and soft plastic PU are made of PU. The loss factor of the SMRM is slightly lower than that of the MRP because the energy dissipation mainly comes from the segment movement of the matrix. Since the cross-linking degree of the sponge is much better than the soft plastic PU, the movement of the segment in the sponge is harder than in the matrix. As a result, the sample with the PU sponge shows a slightly lower loss factor than does the contrast MRP.

In this work (figure 10), the SMRM was tested under different temperatures to study the temperature dependency of the mechanical properties. It can be observed that the G' decreases as temperature increases. The PU is a sort of temperature-dependent viscoelastic material, and it will become softer by increasing the temperature; thus, the G' decreases with temperature. The temperature has little effect on ΔG because ΔG is mainly caused by the dipole-dipole interaction induced by the magnetic field.

Figure 10(b) shows the damping property of SMRM under different magnetic fields, which indicates the loss factor decreases as the temperature increases. When the magnetic field strength exceeds 200 mT, the loss factor curves of the SMRM with different CI content are quite similar. When increasing the temperature, the plastic PUs become soft; thus, the CI particles tend to move easier in the matrix and then the sliding friction between the CI particles and the matrix decreases. Based on this analysis, it can be found that the loss

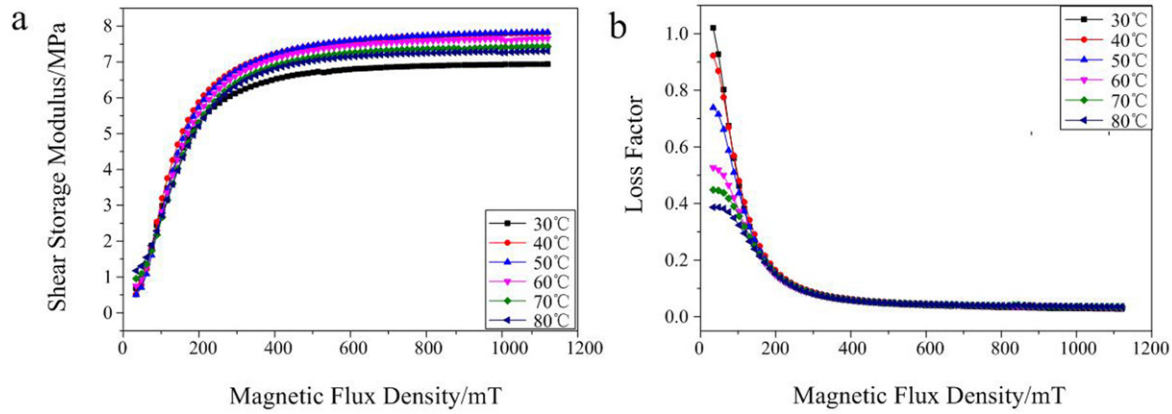

Figure 10. Shear storage modulus of sample with CI content of 60% under different temperatures and magnetic fields.

factor became smaller in the second stage when increasing the temperature.

4. Conclusions

This work demonstrated a novel high-performance MR material in which the stretchable 3D PU sponge was first applied as the matrix to strengthen the PU-CI plastomer. The magnetic-induced modulus of the composite MR material is 7.34 MPa, which is much higher than the MRP. The MR effect can reach as high as 820% when the CI particle content is 80 wt%. The CI particles spread homogeneously in the matrix, and nearly no particle aggregation can found in the matrix. The loss factor finally reduces to as low as 0.03 when the CI particles reach a steady state under the magnetic field, which is much lower than the MREs. In comparison to traditional MR materials, the new SMRM shows flexible, stretchable, and randomly bendable properties; unique damping property; and high magneto-sensitivity under the magnetic field, which would widen the application of MR materials.

Acknowledgments

Financial support from the National Natural Science Foundation of China (Grant No. 11125210, 11102202), the National Basic Research Program of China (973 Program, Grant No.2012CB937500), and the Anhui Provincial Natural Science Foundation of China (1408085QA17) is gratefully acknowledged.

References

[1] Yoshioka H, Ramallo J and Spencer J B 2002 'Smart' base isolation strategies employing magnetorheological dampers *J. Eng. Mech.* **128** 540–51
[2] An J and Kwon D S 2003 Modeling of a magnetorheological actuator including magnetic hysteresis *J. Intel. Mat. Syst. Str.* **14** 541–50
[3] Bica I 2011 Magnetoresistor sensor with magnetorheological elastomers *J. Ind. Eng. Chem.* **17** 83–9
[4] Pinkaew T and Fujino Y 2001 Effectiveness of semi-active tuned mass dampers under harmonic excitation *Eng. Struct.* **23** 850–6
[5] Hoang N, Zhang N and Du H 2011 An adaptive tunable vibration absorber using a new magnetorheological elastomer for vehicular powertrain transient vibration reduction *Smart Mater. Struct.* **20** 015019
[6] Ge L, Gong X L, Fan Y C and Xuan S H 2013 Preparation and mechanical properties of the magnetorheological elastomer based on natural rubber/rosin glycerin hybrid matrix *Smart Mater. Struct.* **22** 115029
[7] Gong Q C, Wu J K, Gong X L, Fan Y C and Xia H S 2013 Smart polyurethane foam with magnetic field controlled modulus and anisotropic compression property *RSC Adv.* **3** 3241–8
[8] de Vicente J, Klingenberg D J and Hidalgo-Alvarez R 2011 Magnetorheological fluids: a review *Soft Matter* **7** 3701–10
[9] Rao P V, Maniprakash S, Srinivasan S and Srinivasa A 2010 Functional behavior of isotropic magnetorheological gels *Smart Mater. Struct.* **19** 085019
[10] Carlson J D and Jolly M R 2000 MR fluid, foam and elastomer devices Mechatronics *Mechatronics* **10** 555–69
[11] Popp K M, Kröger M, Li W H, Zhang X Z and Kosasih P B 2010 MRE properties under shear and squeeze modes and applications *J. Intel. Mat. Syst. Str.* **21** 1471–7
[12] Farshad M and Le Roux M 2005 Compression properties of magnetostrictive polymer composite gels *Polym. Test.* **24** 163–8
[13] Xu Y G, Gong X L, Xuan S H, Zhang W and Fan Y C 2011 A high-performance magnetorheological material: preparation, characterization and magnetic-mechanic coupling properties *Soft Matter* **7** 5246–54
[14] Xuan S H, Zhang Y L, Zhou Y F, Jiang W Q and Gong X L 2012 Magnetic Plasticine™: a versatile magnetorheological material *J. Mater. Chem.* **22** 13395–400
[15] Hodlur R M and Rabinal M K 2014 Self assembled graphene layers on polyurethane foam as a highly pressure sensitive conducting composite *Compos. Sci. Technol.* **90** 160–5
[16] Xu Y D, Cheng L F, Zhang L T, Yin H F and Yin X W 2001 Mechanical properties of 3D fiber reinforced C/SiC composites *Mat. Sci. Eng. A-Struct.* **300** 196–202
[17] Xie X, Yu G H, Liu N, Bao Z N, Criddle C S and Cui Y 2012 Graphene-sponges as high-performance low-cost anodes for microbial fuel cells *Energ. Environ. Sci.* **5** 6862–6
[18] Jin L, Wang H and Yang Y J 2013 Polyurethane composites in-situ molecularly reinforced by supramolecular nanofibrillar aggregates of sorbitol derivatives *Compos. Sci. Technol.* **79** 58–63
[19] Chawla N, Ganesh V and Wunsch B 2004 Three-dimensional (3D) microstructure visualization and finite element modeling of the mechanical behavior of SiC particle reinforced aluminum composites *Scripta mater.* **51** 161–5
[20] Chen W, Rakhi R, Hu L B, Xie X, Cui Y and Alshareef H 2011 High-performance nanostructured supercapacitors on a sponge *Nano lett.* **11** 5165–72
[21] Veedu V P, Cao A Y, Li X S, Ma K G, Soldano C, Kar S, Ajayan P M and Ghasemi-Nejhad M N 2006 Multifunctional composites using reinforced laminae with carbon-nanotube forests *Nat. Mater.* **5** 457–62
[22] Guénon V A, Chou T W and Gillespie J W Jr 1989 Toughness properties of a three-dimensional carbon-epoxy composite *J. Mater. Sci.* **24** 4168–75
[23] Jeong G S, Baek D H, Jung H C, Song J H, Moon J H, Hong S W, Kim I Y and Lee S H 2012 Solderable and electroplatable flexible electronic circuit on a porous stretchable elastomer *Nat. Commun.* **3** 977–81
[24] Yao H B, Ge J, Wang C F, Wang X, Hu W, Zheng Z J, Ni Y and Yu S H 2013 Graphene-polyurethane sponge based on fractured microstructure design *Adv. Mater.* **25** 6692–8
[25] Ge J *et al* 2013 Stretchable conductors based on silver nanowires: improved performance through a binary network design *Angew Chem. Int. Edit.* **52** 1654–9
[26] Scarpa F and Smith F 2004 Passive and MR fluid-coated auxetic PU foam-mechanical, acoustic, and electromagnetic properties *J. Intel. Mat. Syst. Str.* **15** 973–9
[27] Cen H, Kang Y L, Lei Z K, Qin Q H and Qiu W 2006 Micromechanics analysis of Kevlar-29 aramid fiber and epoxy resin microdroplet composite by Micro-Raman spectroscopy *Compos. Struct.* **75** 532–8
[28] Fang F F, Choi H J and Jhon M S 2009 Magnetorheology of soft magnetic carbonyl iron suspension with single-walled carbon nanotube additive and its yield stress scaling function colloids surf A: Physicochem *Eng. Asp.* **351** 46–54